MIGRATION OF LOW ALTITUDE CLOUDS WITH RETREAT OF MARTIAN SOUTH POLAR SEASONAL CO_2 ICE CAP: WHERE DOES ANNUAL ACCUMULATION TAKE PLACE?

I. B. Smith and A. Spiga, *Université Pierre et Marie Curie and Laboratoire de Météorologie Dynamique isaac.smith@lmd.jussieu.fr*

Introduction: Mars' polar layered deposits (PLD) are composed of primarily water ice and dust [1]. The PLD comprise the majority of surface ice on Mars, rising above the surrounding terrain ~3 km, and are together comparable in volume to the Greenland ice sheet on Earth [2]. Both the north PLD (NPLD) and south PLD (SPLD) undergo seasonal variability, especially between winter (when CO2 ice frost covers the polar regions) and summer (when the CO2 ice has sublimed, and water ice and dust are left on a majority of the surface) [3].

The surfaces of the PLD have enigmatic medium scale features, such as spiral troughs, which potentially contribute to understanding both the history of the PLD and the water cycle on Mars [4]. Here we provide evidence that SPLD features, like those on the NPLD, are the result of persistent katabatic winds that contain katabatic jumps. NPLD features related to winds have been studied in detail [4,5, 6], yet few studies have attempted to relate the landforms on the SPLD to modeled winds [7].

Recent evidence on the NPLD has shown that the spiral troughs likely formed within a constructional setting, with winds and atmospheric deposition likely playing the major roles [4, 8]. Observations of low altitude clouds and atmospheric modeling [4], surface morphology [9], in addition to radar stratigraphy [8] demonstrate that ice is transported across the NPLD by wind to form and modify these features, but no studies have have combined the same observations and modeling for the SPLD.

Here we expand previous work on the NPLD [4] to the SPLD. We utilize observations of surface morphology, topography, subsurface stratigraphy, and near surface clouds, in combination with mesoscale simulations of south polar winds and temperature, to investigate processes governing the accumulation and retention of ice on the south pole of Mars

Methods: As of this writing, more than 14,200 visible wavelength Thermal Emission Imaging System (THEMIS) images that capture portions of the SPLD are publicly available. We analyze the majority of these images to find near surface trough clouds (Figs. 1 and 2). To garner the best possible statistics, THEMIS visible observations are examined from six mars years: MY26, MY27, MY28, MY29, MY30, and MY31. The Mars Orbital Camera (MOC) wide angle camera also detects trough clouds as early as in MY25. The SPLD is not symmetric about the south pole, so regions of interest include everything south of -80°, and between -80° and -71° for longitudes 90° to 220° (Fig. 3). Our sampling includes dates from L_s 190° to L_s 330° for all of the SPLD (Fig. 4). L_s is the angle of orbit around the sun, starting with $L_s = 0$ for northern vernal equinox.

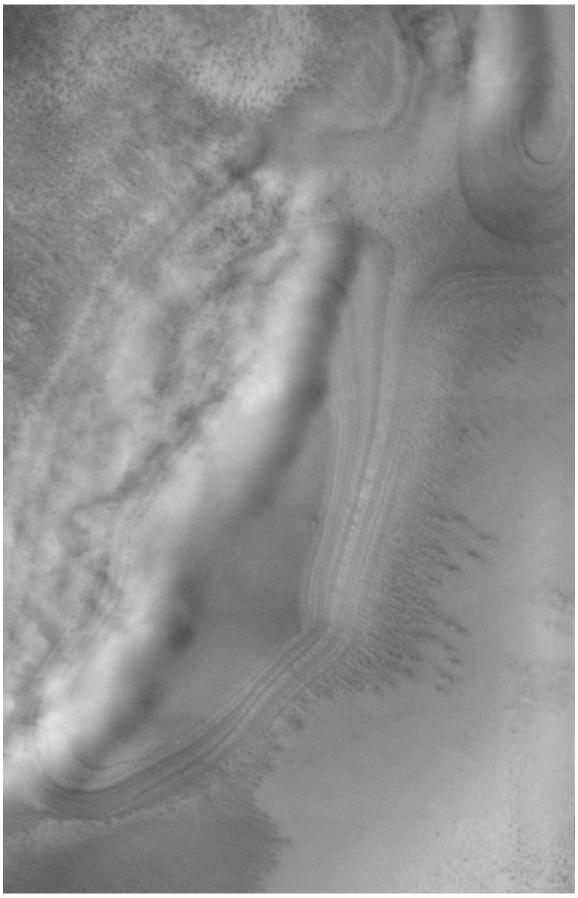

Fig. 1. *THEMIS VIS image V07272010 exhibiting a trough cloud that results from a katabatic jump in Region 1. Clouds is found just above the lowest portion of the trough.*

To simulate atmospheric conditions on the SPLD, we use a mesoscale model developed at the Laboratoire de Meterologie Dynamique (LMD) [10]. Model simulations for the SPLD are comparable to those that have been conducted on the NPLD [4, 6, 11]. Wind speed, wind direction, and temperature are output every hour for an equally divided "24 hour" Mars day. We simulate the conditions at several dates throughout spring and summer: including L_s 230°, 260°, 290°, and 330°.

Our simulations cover the entire SPLD and surrounding regions: ~1800 km by 1800 km centered on 86° south and 173° east. The grid is 101 by 101 cells, yielding a resolution of ~18 km per cell. At this resolution the general topography of the SPLD is represented, but smaller features are not present.

To model near-surface winds, it is particularly important to account for the evolution of the seasonal CO_2 ice deposit. As was shown e.g. by [12 and

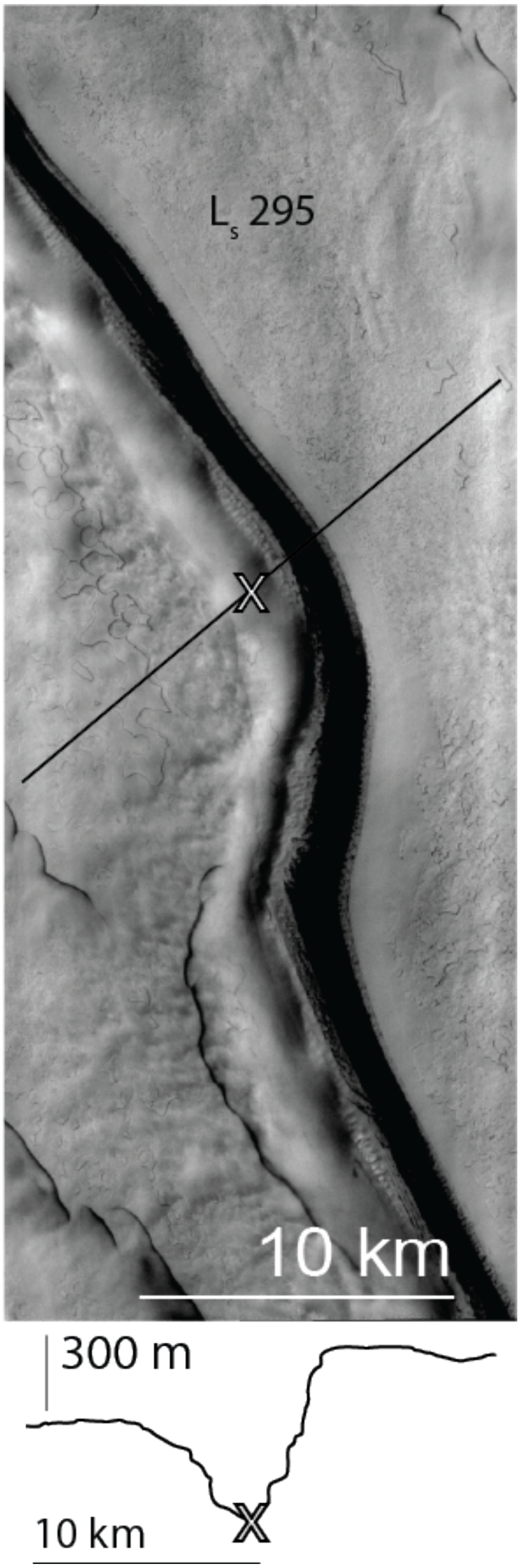

Fig. 2. THEMIS VIS image V41808006 exhibiting a trough cloud in Region 4. Clouds is found just above the lowest portion of the trough and later than clouds in other regions.

13], near-surface regional winds over Martian polar caps are controlled both by topography and surface temperature, hence CO_2 ice deposits, which fix the surface temperature to below 150 K (Fig. 5). Our mesoscale simulations therefore use a prescribed CO_2 seasonal deposit that evolves by L_s date according to infrared measurements of the surface temperature [3]. We use the analytical functions provided by that study to obtain the crocus line, i.e. the external boundary of seasonal CO_2 ice deposits (named after a crocus flower that blooms as ice recedes).

Observations: Trough clouds are detected over large ranges of latitude, elevation, and date. Spatially, trough clouds are found at all latitudes of the SPLD, from -71° to 89°S. They manifest near topographic changes, especially where slopes decrease (near the bottom of troughs (Fig. 1). Trough clouds are observed as early as L_s 198, and as late as Ls 318 (Figs. 3 and 4) for a total seasonal range of ~120° L_s, far greater than the ~60° of L_s on the NPLD [4].

Trough clouds are detected at locations that vary spatially in correspondence to date (Figs. 3 and 5 m1-m4). We divide the SPLD into four regions based on the timing, latitude, and elevation of detected clouds (Fig. 3). In general, clouds at lower latitudes occur earlier in the spring, and clouds of higher latitudes appear later. Based on THEMIS VIS images, Regions 1 through 4 each contains 80, 64, 89, and 231 observed clouds, respectively (Fig. 3).

Region 1 corresponds to Ultimi Lingula, between 120° - 235° E and 70° - 83.5° S (Fig. 3). Clouds are observed throughout 44° of L_s (Fig. 4), and this region sees the most activity in the early part of the cloudy season.

Region 2 resides from 85° to 110° E and 85.5° to 87°S, distinguished by its location at the head of Chasma Australe (Fig. 3). The 64 cloud detections span from L_s 225° through 268° (Fig. 4), during a transition period between Regions 1 and 3.

Region 3 experiences trough clouds over a longer duration than other regions. It resides higher in latitude than Region 1, between 80° and 86.5° S, and extends over an enormous elevation range (~3500m). Longitudinally, Region 3 spans 5° to 110°E (excluding Region 2). The majority of Region 3 clouds are observed between L_s 241° and 295°, for a duration of 54°, while 6 clouds are detected earlier (Fig. 4).

Finally, Region 4 primarily contains Australe Mensa and the residual CO_2 ice cap but extends to the margin near 83° (Fig. 3). All detections of trough clouds after L_s 290° are found in Region 4, for a total of ~170 images. The remaining ~ 60 detections are as early as L_s 250°, with 55 imaged between L_s 265° and 286°. The majority of Region 4 trough clouds are at high latitudes and between L_s 265° and 318°, the last date of observed clouds on the SPLD.

The four regions were delineated based on timing and location, but there are some regions in which no clouds are observed, including a dearth of detections in Promethei Lingula (except near the head of Chasma Australe) and Australe Scopuli. Furthermore, no trough clouds are found in the vast, smooth plains between Australe Mensa and Ultima Lingula.

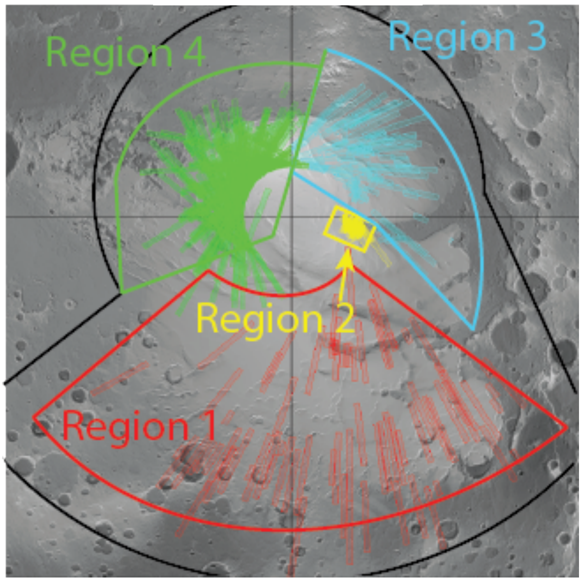

Fig. 3. *SPLD basemap showing color coded footprints of THEMIS cloud detections and regional delineation. Colors match Fig. 4. Black border depicts survey area. Over 500 SPLD clouds are found.*

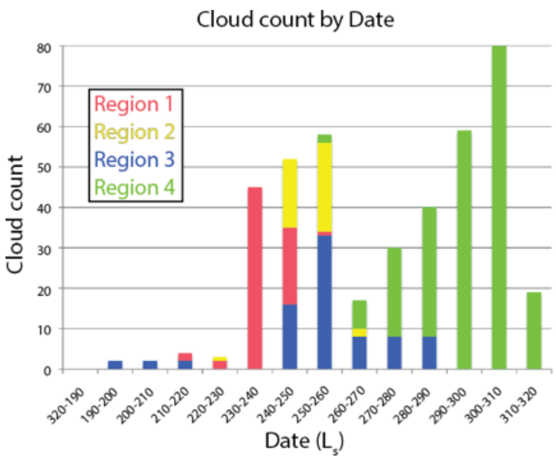

Fig. 4. *Histogram of detected clouds by date. Colors correspond to Regions 1 through 4. Most clouds before L_s 240° are within Regions 1 and 2. All clouds found after L_s 290° are detected in Region 4.*

This disparity between where clouds are found and where they are absent demonstrates the localization of cloud formation on the SPLD.

Overall, there is a southward progression of detected clouds (Fig. 5 m1-m4). Between date ranges L_s 220° and 230° all but one cloud is found in Region 1. Dates between L_s 250° and 257° have no clouds in Region 1, but many are found in Regions 2 and 3. Region 4 has a few detections, primarily at the SPLD margin. Between L_s 280° and 300°, the majority of clouds are in Region 4, with only a few in Region 3. Eventually, after L_s 320°, no clouds are detected. This progression follows the measured crocus line of CO_2 ice (Fig. 5 t1-4) [3].

SPLD mesoscale model: Using mesoscale simulations described in Methods, we map surface temperature and wind vectors 20 m above the SPLD surface. Simulations show that near-surface winds undergo a moderate daily cycle, so we focus our analysis on comparing winds at various seasons for a fixed local time, 23h (Fig. 5).

On a seasonal basis, the fastest winds on the SPLD are often found in the vicinity of the crocus line. As the season progresses and the seasonal cap retreats towards the pole, so do the fastest winds (Fig. 5 t1-t4). This is consistent with the mesoscale simulations of [13], who found that the cap-edge thermal contrast yielded high surface wind stresses likely to give birth to high dust storm activity [14].

The physical mechanism for thermal circulations is well-known on Earth with "sea-breeze" circulations. Thermal surface heterogeneities in a given region (e.g. ground CO_2 ice near bare soil on Mars) lead to regional temperature gradients. Through hydrostatic equilibrium, this in turn leads to regional pressure gradients. Thermally-direct circulations arise, with deflection by the Coriolis force possible.

Our mesoscale simulations support evidence that SPLD regional circulation in the vicinity of the crocus line boundary likely results from a combination of cap-edge circulations and slope winds [12]. The topographical heights of the SPLD primarily drives slope-wind (katabatic) circulations, as is the case for most regions on Mars featuring uneven topography, e.g. [11]. This existing circulation is reinforced by an additional thermally-direct circulation analogous to the sea-breeze circulation on Earth. The combination of those two kinds of regional circulations in driving the near-surface winds explains why enhanced winds are mostly found in the vicinity of the crocus line, but not necessarily at the precise location.

The simulation for L_s 290° is maybe the most illustrative example of this combination (Fig. 5 t3). The crocus line is located so that the slope winds produced by the SPLD topographical summit is optimally enhanced by thermally-direct circulations caused by the nearly 100 K contrast between surface temperature above the CO_2 seasonal cap and the lower-latitude dusty terrains. Near-surface winds can reach speeds approaching 20 ms^{-1}. Later in the season, at L_s 320°, the temperatures outside the crocus line are cool enough that the cap-edge thermal contrast is significantly reduced, causing no near-surface winds to be predicted above 10 ms^{-1} in the model.

Yet, while this scenario is supported in most cases shown in Fig. 5, the relationship between strong winds and trough clouds is less clear at L_s 230°. Near Australe Mensa the winds are modeled to be extremely fast, and divergent from the pole, while no trough clouds are detected. This reminds us that strong winds conducive to the formation of katabatic jumps are a necessary but not sufficient condition for trough clouds. Those clouds need the water vapor mixing ratio in the atmosphere to be high enough to form. It is very likely that the cold trap of ground water ice by seasonal CO_2 ice (e.g. [15]) is very effective on Australe Mensa at L_s 230°, which would account for low water vapor mixing ratios in the atmosphere, and consequently no trough clouds will form.

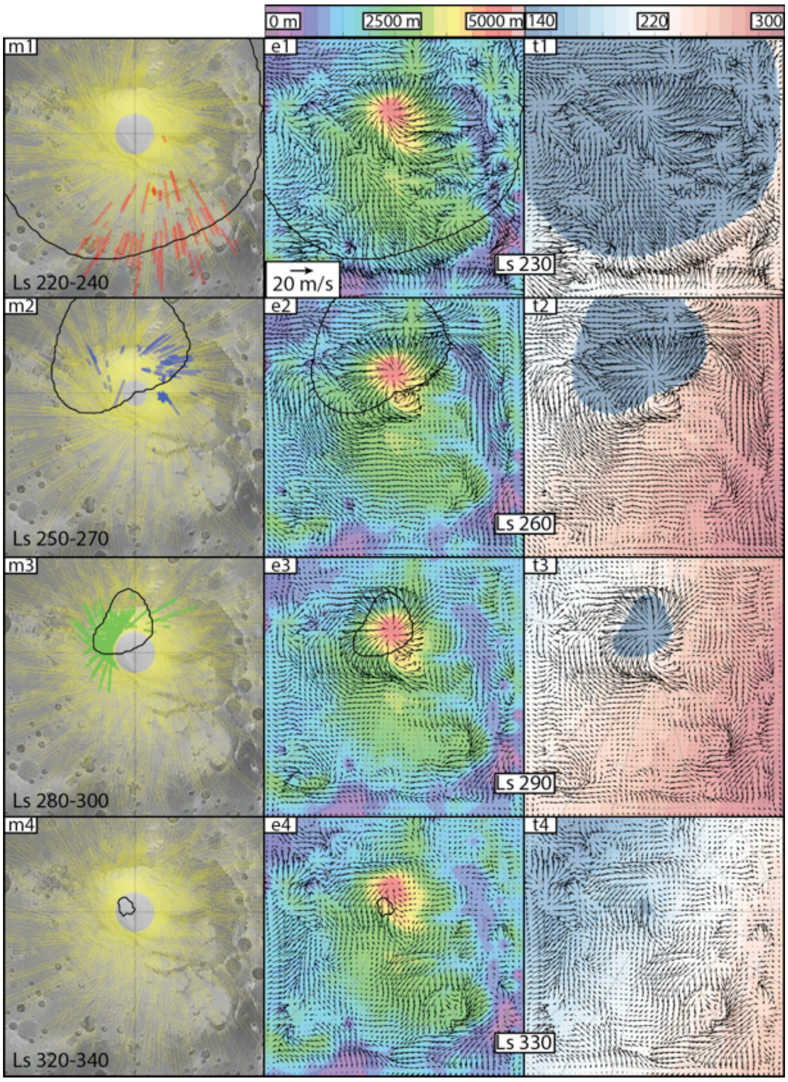

Fig. 5. *Maps of SPLD for cloud detections and wind speeds corresponding to topography and temperature. m1 – m4: Cloud detections (in red, blue, and green) overlaying available THEMIS image footprints (yellow). A plethora of observations are available, 220°-240°: 3093; 250°-270°: 2710; 280°-300°: 2152; and 320°-340°: 2169. Cloud detection is not limited by coverage. There is a poleward progression of cloud detections as date increases. Solid black line corresponds to the crocus line, or line of CO_2 seasonal ice extent. e1 – e4: Map of SPLD wind vectors 20 m above the surface overlying colorized topography. Winds generally have higher velocities near strong slopes. t1 – t4: Map of SPLD wind vectors 20 m above the surface and surface temperature. CO_2 seasonal ice retreats as the season progresses, along with the ~148 K fixed surface temperature [3]. The highest wind speeds on the pole are found near the greatest temperature contrast, at the crocus line. Clouds are detected where strong thermal contrasts meet with steep slopes and high water vapor content.*

Conclusions: Our mesoscale atmospheric simulations demonstrate that winds are very fast near the boundary between the seasonal CO_2 crocus line and the exposed, underlying, permanent ice cap. As this crocus line retreats poleward during spring and summer, so do the fast winds. Where the winds are fastest and water vapor availability is high, katabatic jumps (and trough clouds) are expected to form. Our observations of cloud appearances matches well with the location of the crocus line and fastest winds.

We find that winds have played a major role in determining where ice accumulates on the SPLD . This work, in combination with detailed subsurface stratigraphic analysis [16] indicate that sites of deposition and retention of ice on the pole coincide with where clouds form. In this way, clouds influenced by the retreating CO2 seasonal cap tell us where annual and long-term accumulation occurs. Thus, it is possible, and eventually testable with adequate modeling, that trough morphology is interdependent on a seasonal CO2 ice cap and that the troughs themselves may require a seasonal cap to initiate. Future work will test this hypothesis.

This work is being extended to determine if a similar spatial pattern of clouds and crocus line is detected at the NPLD. Initial results show that clouds are detected over a much shorter range of Ls dates and over a smaller spatial scale. This will also be presented at the meeting

Acknowledgements: This work was supported by NASA ESSF Fellowship NNX10AT24H, NASA MDAP grant NNX10AO26G, the Jackson School of Geosciences, and the William J. Fulbright Foundation. We thank the SHARAD science team and Arizona State University's JMARS software and web-based Mars Image Explorer.

References: [1]Grima, C., et al. (2009), *GRL*, *36*(3), L03203. [2] Smith, D. E., et al. (2001), *JGR Planets*, *106*(E10). [3] Titus, T. N. (2005), *36th LPSC*, Abst. 1993.[4] Smith, I. B., et al. (2013), *JGR Planets*. [5] Brothers, T. C., et al. (2013), Mars, *GRL*. [6] Massé, M., et al. (2012), *EPSL*, *317–318*, 44–55. [7] Koutnik, M. R., et al. (2005), *Icarus*, *174*(2), 490–501. [8] Smith, I. B., & J. W. Holt (2010), *Nature*, *465*(7297), 450–453. [9] Howard, A. D. (2000), *Icarus*, *144*(2), 267–288. [10] Spiga, A., & F. Forget (2009), *JGR.*, *114*(E2), E02009. [11] Spiga, A., et al. (2011), *Icarus*, *212*(2), 504–519. [12] Siili, T., et al. (1999), *PSS*, *47*(8–9), 951–970. [13] Toigo, A. D., et al. (2002), *JGR Planets*, *107*(E7), 4–1–4–13. [14] Cantor, B. A., et al. (2001), *JGR*, *106*, 23653–23688. [15] Montmessin, F., et al. (2004), *J. Geophys. Res.*, *109*(E10), E10004. [16] Smith, I. B., et al. (in review), *Geomorph. Special Issue*.